Powder Technology 415 (2023) 118095

Contents lists available at ScienceDirect

Powder Technology

journal homepage: www.journals.elsevier.com/powder-technology

# Features of near gravitational material tracers in a dense medium cyclone from PEPT

M.C. Richter [a,*], A.N. Mainza [a], I. Govender [a,b,c], N. Mangadoddy [d], R. Sivakumar [e], G.E. Sreedhar [e], M.R. van Heerden [f,g]

[a] Centre for Minerals Research, Department of Chemical Engineering, University of Cape Town, Rondebosch 7460, South Africa
[b] School of Engineering, University of KwaZulu Natal, Howard College, Glenwood, 4041, South Africa
[c] Mintek, P/Bag X3015, Randburg, Gauteng 2121, South Africa
[d] Department of Chemical Engineering, Indian Institute of Technology Hyderabad, Kandi 502285, Telangana, India
[e] R&D, National Mineral Development Corp. Ltd., Uppal, Hyderabad 500007, Telangana, India
[f] PEPT Cape Town, Department of Physics, University of Cape Town, South Africa
[g] iThemba LABS, Somerset West 7129, South Africa

## HIGHLIGHTS

- labeled coal NGM particle trajectory in 4in operating DMC imaged using PEPT
- resolve axial variability of two-vortex model at cyclone boundary transition
- locus of zero vertical velocity captured
- quantified turbulence distribution of NGM particle trajectories
- demonstrate axial velocity model fit

## GRAPHICAL ABSTRACT

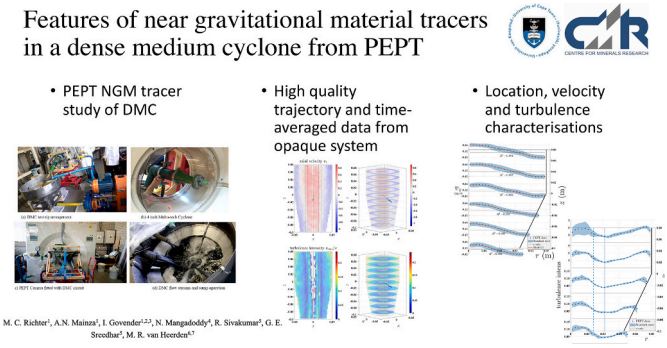


## ARTICLE INFO

*Keywords:*
Dense medium cyclone
Near-gravity material
PEPT
Flow field
Turbulence

## ABSTRACT

Dense media cyclones are an integral part of circuits employed for coal processing, iron ore beneficiation, and recovery of diamonds. Many techniques have been applied in studying the separation performance of these devices including the use of different density tracers to develop density partition curves. This study focusses on tracking of near-gravity material radioactive tracers using the positron emission particle tracking technology. This near-gravity phase of coal has long been thought to cause separation inefficiencies which makes coal processing difficult. In this work, a slurry containing magnetite-based dense medium, and coal is pumped through a 100 mm Multotec cyclone. By means of the PEPT camera – apparatus with spatial and temporal resolutions of 1 mm and 1 ms respectively – and direct-adsorption-activated coal tracer particles within the medium, particle trajectories are recorded in space and time. The free vortex region is captured and shown to fit the Rankine vortex behaviour with $n = 0.60 \pm 0.08$ overall for the free vortex power law decay. A logarithmic axial velocity model which captures the observed radial gradient around the locus of zero axial velocity is

* Corresponding author.
*E-mail address:* mc.richter@uct.ac.za (M.C. Richter).

https://doi.org/10.1016/j.powtec.2022.118095
Received 17 June 2022; Received in revised form 17 October 2022; Accepted 10 November 2022
Available online 14 November 2022

proposed. Radial profiles of turbulence intensity for the near gravitational material as captured by PEPT are presented.

## 1. Introduction

Cyclones have been used in the mining industry for the separation of different classes of particles according to size, density, and shape. They are commonly used in the minerals processing industry to control the classes of particles that can exit the comminution circuits and report to the recovery process downstream. They are preferred in the minerals industry because they can handle high capacities, can tolerate a wide range of operating conditions, and can be installed on a relatively small footprint. A feed mixture containing particles of different size and density classes is introduced in the cyclone separator at high pressure into an axially symmetric vessel resulting in high tangential velocities of the particles, or swirling flow that leads to separation of particles based on inertia and viscous forces. High inertia particles which comprise larger and heavier particles move towards the wall of the cyclone body while low inertia particles consisting of smaller and lighter particles orbit at smaller radii near the center of the vessel under the influence of viscous forces. The larger and heavier particles orbiting at large radii near the wall experience momentum loss through friction with the cyclone wall and gradually move axially towards the spigot orifice and exit as underflow stream. Many common designs, such as for instance hydrocyclones, dense medium cyclones, thickening cyclones, and liquid-liquid cyclones, have a conical section that narrows towards the spigot and the underflow stream crowds out the available space at the spigot, where a flow reversal forms into a forced vortex. Smaller and lower density particles that are oriented closer to the forced vortex in the cyclone body and are carried by the upward-moving swirling flow towards the overflow discharge [1,2]. For a set up that has the overflow and underflow discharge orifices open to the atmosphere, a central vortex air column spanning from underflow to overflow exit orifices forms.

Dense media cyclones (DMC) are widely used in coal preparation, and are also used as the primary concentration step in the recovery of diamonds, iron ore concentration, pre-concentration of base metals, and some industrial minerals [3]. DMC uses centrifugal sedimentation to separate particles based on density difference with respect to the dense media. It provides very efficient separation compared to other gravity processing methods, especially when the near gravity material is above 10% [4,5]. The medium that is added allows the DMC to achieve separation at desired density cut-points.

In coal washeries, coal particles mixed with magnetite slurry in the volume ratio (medium to coal) of 4:1 is injected tangentially into the cyclone. Like hydrocyclones, in DMC due to the centrifugal force, heavier/high-density ash particles are transported towards the wall and are discharged through the underflow by a primary free vortex motion. Lighter/low-density coal particles remain in the liquid near the center and are discharged through the overflow stream following a forced vortex motion. As both outlets are open to atmospheric launders/ducts, a low-pressure region is created at the center, generating the air-core. The presence of different sizes and densities of magnetite and coal particles along with water and the air-core in a highly turbulent Rankine vortex makes the DMC flow very complex.

There have been many investigations to understand the physics of the swirling flow and particle dynamics through the assessment of particle separation by experimental techniques, by both theoretical and semi-empirical approaches. In due course, regression models based on data collected from the pilot and plant-scale DMCs became more successful in predicting process performance for process design and optimization. Notable contributions on mathematical models for coal partitioning [6] and for coal and mineral separations [7] are noted here.

While the shape and construction of cyclones is relatively simple, the internal features of the fluid flow are more complex. Most evaluations of cyclone performance are more broadly empirical and leave room for advancement of theoretical models, based on fundamental measurement of particles inside the system. This form of modelling is desirable, as an inquiry based on an exclusively empirical approach is limited in its capacity for optimization and innovation. A reason for such a lag in fundamental theoretical description may be the limited measurement tools available for the characterisation of the flow fields within such systems. With ever more research covering the fields of particle tracking as it pertains to systems like a hydrocyclone, such as particle image velocimetry (PIV) [8], laser Doppler anemometry (LDA) [9,10] more sophisticated models have become achievable. The alternate tracking technique called positron emission particle tracking (PEPT) promises an improved technique for in-situ high precision trajectory tracking within an opaque slurry system. The formerly mentioned techniques represent Eulerian time-averaged velocity flow fields, while the PEPT approach can also yield Lagrangian type data of individual particle trajectories and their behaviour at a different timescale within the flow. This aspect makes PEPT a desirable tool in the study of the generalised cyclone system and has been used in several projects related to minerals processing applications that range from mixing vessels [11] [12] and fluidised beds [13] to tumbling mills [14] [15] and floatation cells [16,17]. Hydrocyclones have also been successfully imaged using PEPT [18–20].

Limited studies are available on the flow field [21] and medium segregation [22,23] measurements inside the DMC using experimental techniques such as gamma ray tomography (GRT), X-ray tomography and sampling probe used for mapping the particle density/concentration inside the DMC. Usage of empirical [24,25] and analytical modelling approaches [26,27] are limited for predicting the performance characteristics in DMC because of their inherent assumptions. But precise experimental measurements of particle & fluid velocity and air-core are difficult and very sparse literature is available as of today. The computational techniques, such as computational fluid dynamics (CFD) based on continuum mechanics principles and control volume methods for turbulence and multiphase flow predictions are evolved as a matured technology after the decades of dedicated and continuous research [28].

Early 2D computational models [29,30] required imposing a fixed air-core size to model shear-based wear rates at the vortex finder. 3D multiphase simulations [31] extended this modelling approach with a single average particle size representing the magnetite phase dispersed in water in a 350 mm DMC with the standard mixture model [32] available in ANSYS's Fluent, computing the air core by means of a mixture model treating air as an additional dispersed phase unlike the fixed air-core size approach.

Subsequent improvements to CFD modelling [33] incorporated particle size distribution, slip velocity in the mixture model modified with shear lift forces, and slurry rheology modeled by [34] using a Newtonian viscosity relation into the flow medium. Furthermore, the effect of magnetite particle size distribution on the flow behaviour was studied and it was observed that fine particles were distributed throughout the cyclone while coarse particles clustered densely near the wall. [35] studied the flow characteristics in a 350 mm DMC using a mixture multiphase model modified with a viscosity correction factor and DPM for coal particle tracking.

The particle scale modelling approach using discrete element modelling (DEM) of particles and coupling it with CFD model of the carrier fluid flow has also been attempted [36]. Several key operating parameters such as the effect of particle density [37], solid loading [38], fluctuations in mass flowrate [39] have been studied using the coupled CFD-DEM model. The major drawback that has limited this more fundamental modelling approach is the computational requirement

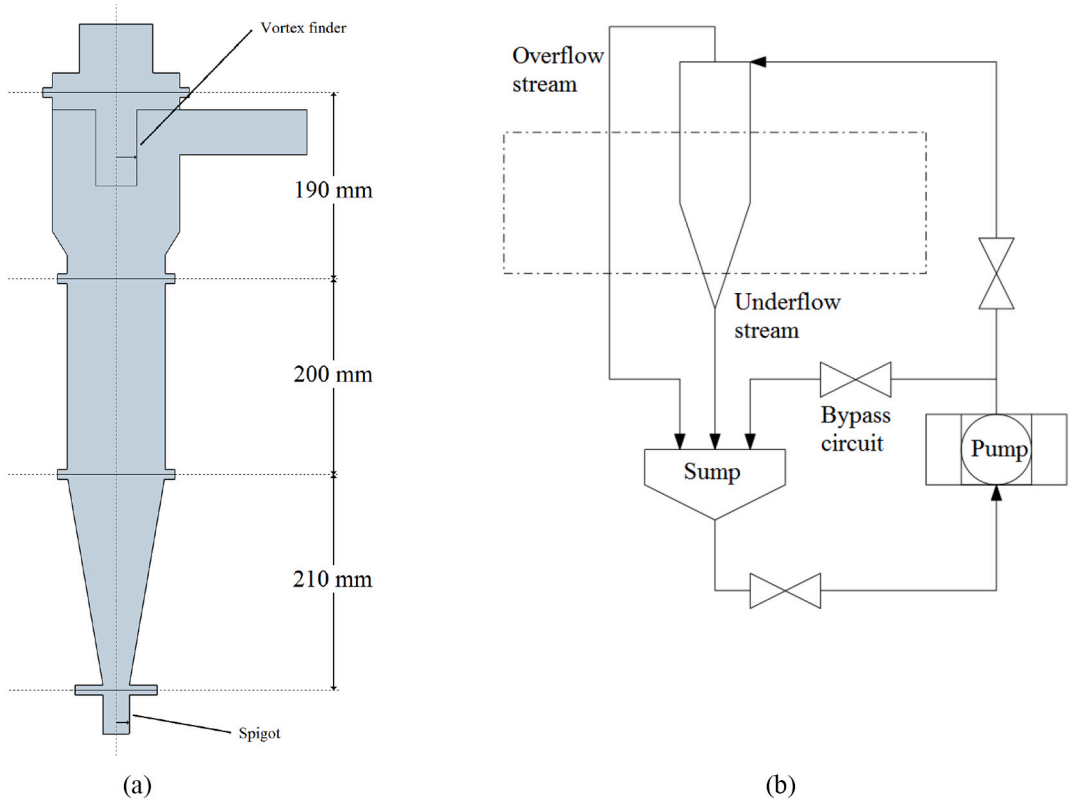


**Fig. 1.** (a): Schematic of cyclone body. Fig. 1 (b): Diagram of flow circuit to operate the dense medium cyclone within the PEPT camera field of view as depicted from above.

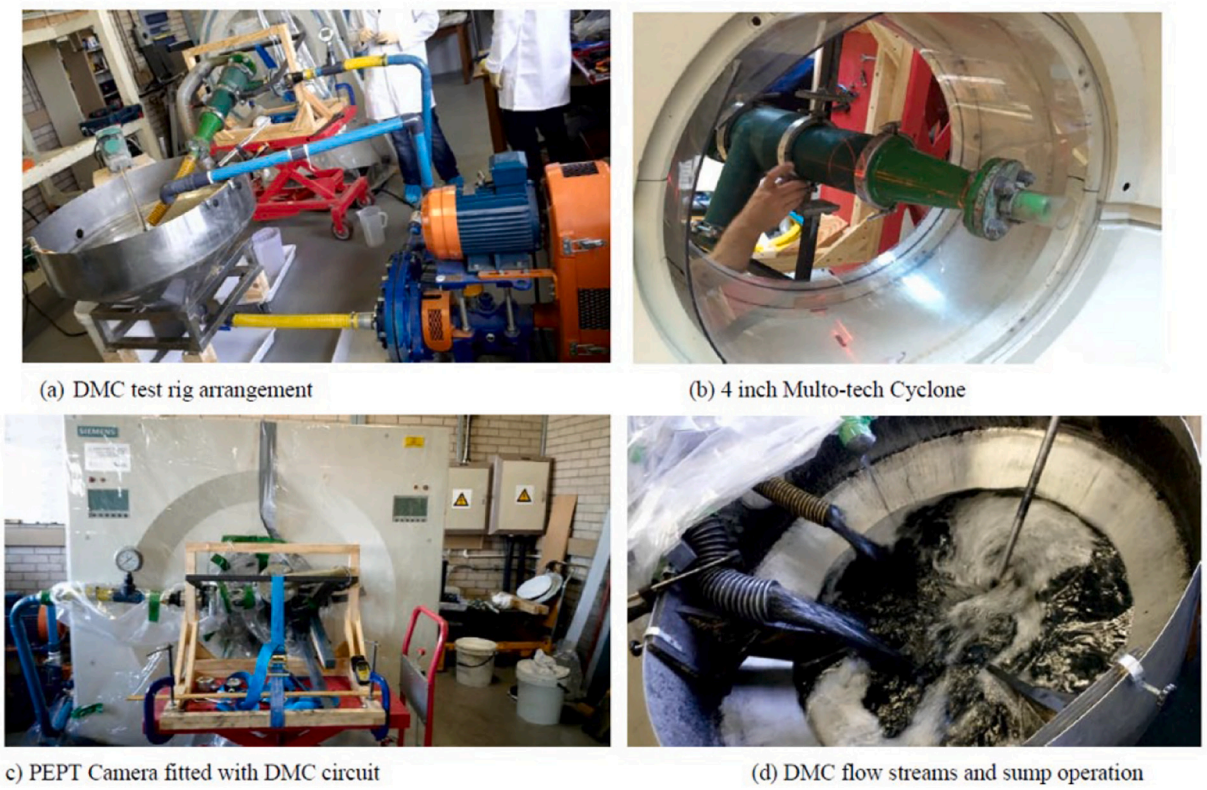


**Fig. 2.** Images showing the laboratory and test rig used to track particles inside a dense medium cyclone and illustrating the orientation of the cyclone within the detector.

**Table 1**
Density distribution of bituminous coal used in dense medium cyclone PEPT experiments.

| Coal Density | (g/cm$^3$) | 1,30 | 1,35 | 1,40 | 1,45 | 1,50 | 1,55 | 1,60 | 1,65 | 1,70 | 1,75 | 1,80 | 1,85 |
|---|---|---|---|---|---|---|---|---|---|---|---|---|---|
| Cumulative Distribution | (%) | 0,0 | 3,7 | 8,2 | 16,3 | 25,2 | 34,8 | 44,1 | 50,6 | 56,8 | 61,6 | 69,3 | 100 |

associated with tracking each particle in the dense particulate flow system. The above-listed studies have used DEM only to model coarser coal particles of the size range (0.5–5 mm), while micron-scale particle tracking remains computationally intractable. Another important factor determining computational requirements is the choice of turbulence models. [40] discussed the applicability of Reynolds stress model (RSM) for large scale cyclones where turbulence levels are small. Recently, a 3D GPU algebraic slip mixture (ASM) model coupled with large eddy simulations (LES) were developed [41] for modelling the medium segregation of DMC and found that with parallel GPU computation one could achieve around 13 times simulation speed-up for the multiphase case as compared to the CPU computation.

The novelty of this investigation lies in the specific study of near-gravity material (NGM) as it traverses a DMC treating fine coal in a magnetite medium and the information that can be extracted from the trajectories tracked using the PEPT technique. [19] [20]. The common definition of material as NGM is that fraction of coal present within the separation medium that falls within a density range of ±0.1 of the separation density of the DMC [42], although for coal with much higher concentrations of ash, motivation for a narrower range exists [43]. While bulk behaviour of such particles has been previously known, information from individual trajectories moving through the cyclone body has been largely unknown. It is hypothesised that this NGM is an important driver of the frequently observed misplacement of feed components to the wrong product stream of the DMC [44], making some coal particles much more difficult to refine to a viable state. Furthermore, simulations that model such complex multicomponent systems and their dynamics rely on CFD, which offers yet more bulk descriptions of behaviour and requires verification. This work aims to propose a non-invasive method for studying the particles with density approximately that of the separation density of the DMC. The effect this NGM has on flow fields and the resulting turbulence is unknown and more such studies are required to quantify and evaluate their impact.

## 2. Cyclone configuration, charge specification, PEPT

### 2.1. DMC flow circuit

The dimensions of the DMC under investigation are shown in Fig. 1 (a) and the schematic of the experimental setup is depicted in Fig. 1(b). The DMC was placed within the Siemens EXACT3D scanner to image the tracer activity in a section of the cyclone body that was within the field of view of the scanner. The cyclone was positioned in such a way that the transition of the tracer from the cylindrical body to the conical section was captured. Further details of the cyclone body include the diameter of $D_c$=100 mm giving inner radial size of $R_c$= 50 mm, inlet diameter of 65 mm, vortex finder diameter of 42 mm, and spigot diameter of 28 mm. These dimensions were chosen to achieve an optimum flow split for the dense medium and sufficient density difference in the outflow stream indicating medium stability at 9 $D_c$ inlet head [6]. The cyclone was suspended across the field of view of the scanner at an angle of 70° raised from vertical. A conical sump of diameter 1 m and maximum operational volume of 150 L received the underflow and overflow streams from the cyclone product streams as well as the bypass circuit. The sump contents were kept in suspension by an agitator and baffles within the sump ensured good mixing and minimal cavitation at the sump exit stream. The whole system was driven by a pump run at 90–93% of its maximum driving frequency to maintain the required operating pressure in the range of 20 to 25 kPa. (See Fig. 2.)

Three variations of dense medium were prepared, composed of mixtures of magnetite ($Fe_3O_4$, $-45\mu m$, and specific gravity of 4.8 g/cm$^3$) in water to achieve feed densities of 1.4, 1.5 and 1.6 g/cm$^3$, respectively. To this medium, coal was added at the proportion of at least 4.5 to 1 medium to coal ratio by volume. The coal contained an ash content of 33.9 ± 0.7%. Density distribution of the coal is shown in Table 1. All coal particles larger than 6.3 mm were discarded and of the remaining material, 25% were smaller than 1 mm, 43% between 1 mm and 3.35 mm and 32% between 3.35 mm and 6.3 mm.

Each batch of dense medium (magnetite slurry) and coal mixture was utilised over 2 days of PEPT data acquisition, resulting in approximately 6 h of operation/processing time per batch of slurry. The coal phase of these slurries was observed to have changed noticeably after this time and a new slurry was then prepared. The mandatory decontamination protocol of samples containing nuclear material contaminants made testing of these degraded slurries unfeasible at the time.

Samples of the over- and underflow streams were taken before the coal phase was added to the medium. One additional stream sampling was performed before the radiolabeled tracer was injected into the sump, after which no further samples were collected during the tracer's active period to ensure the safety of the laboratory team by reducing physical contact with potentially contaminated samples. Once the tracer was added to the medium, no further adjustments to the slurry or pump driving frequency were made.

### 2.2. PEPT technique

The technique of PEPT is well established as a non-invasive determination of the location in 3D space and time of one or more radiolabeled tracers [45]. The radioactive component applied to the traceable particle generates positrons, the positively charged electron antiparticles, because of the nuclear decay of the unstable element. These positrons annihilate with electrons present in the surrounding matter very soon after coming into existence and this produces two gamma rays containing the mass energy of the two massive particles. Thus, each gamma ray (or photon) carries away 511 keV in near co-linear opposing directions from the point of annihilation. An event is logged by the system of electronics when these photons deposit their energies in detectors at opposite ends of the detecting structure (in this case a ring formation) within the window of simultaneity. The two detectors involved in such a triggered event form the line of response (LoR) that is captured by the acquisition system. A trajectory is built from a time series of intersecting LoRs and consequently velocity and higher order derivatives can be extracted from the data. The tracking data were acquired through the Siemens ECAT HR++ EXACT3D tomographic scanner in operation at the PEPT facility at iThemba LABS, in Cape Town, South Africa. This tomograph features a ring geometry of 48 bismuth germanium oxide detectors, providing a cylindrical field of view of 234 mm axial dimension and approximately 250 mm of radial dimension. The nature of the acquisition hardware attached to the detector allows a time resolution of $10^{-3}$ seconds in the received data and spatial resolution of 1 mm, depending on activity of the tracer and attenuating environment. Location markers were used to locate the boundary of the cyclone body and used as reference when the collected PEPT data was analysed. These location markers were radioactive sources affixed to the exterior of the cyclone body and located using the PEPT detector. Thus, the orientation of the cyclone body within the field of view was determined.

Among the various tracking techniques for flow problems, PEPT has many beneficial aspects to exploit in experimental investigations into fluid and granular flow behaviour. The non-invasive nature as well as

**Table 2**
List of properties of tracers and dense mediums produced and tracked in PEPT experiments of the dense medium cyclone operation.

| Tracer ID | Tracer density | Tracer dimension | Density of medium | Initial Tracer activity |
|---|---|---|---|---|
| | ($g/cm^3$) | (mm) | ($g/cm^3$) | (μCi) |
| D1 | 1,37 | 2,2 | 1,00 | 1600 |
| $D2_2$ | 1,47 | 2,1 | 1,44 | 1800 |
| D3 | 1,72 | 2,0 | 1,45 | 1600 |
| $D4_1$ | 1,67 | 2,2 | 1,63 | 1600 |
| $D4_2$ | 1,57 | 2,2 | 1,62 | 1670 |
| $D5_1$ | 1,52 | 0,8 | 1,52 | 1580 |
| $D5_2$ | 1,52 | 1,6 | 1,52 | 1600 |
| D6 | 1,63 | 0,7 | 1,49 | 1320 |
| $D7_1$ | 1,53 | 2,8 | 1,49 | 2150 |
| $D9_1$ | 1,70 | 0,8 | 1,57 | 1360 |
| D10 | 1,43 | 1,0 | 1,39 | 1210 |
| D11 | 1,53 | 1,2 | 1,39 | 1420 |
| D12 | 1,53 | 2,2 | 1,39 | 2970 |

reasonably high precision tracking makes it particularly useful in investigating fluid flow within industrial apparatuses such as industrial cyclones. Such Lagrangian investigations remain pivotal in understanding local behaviour of flow that has complex composition and demonstrates non-linear features. From multiple individual trajectories observed within the fluid flow, long term time-averaged features can be obtained.

#### 2.2.1. Representative tracer production

Tracers produced to represent NGM coal particles within a dense medium separation were used in these tracking experiments. The production process consists of adsorption of $^{68}Ga$ onto carefully selected coal particles within the size classes of interest and coated with a protective cyanoacrylate shell to avoid tracer breakage and minimise radioactive leaching and contamination of the medium or lab apparatus. This coating approach was favoured over an uncoated tracking particle for the two main reasons of lab safety and quality of tracking data, to maximise physical integrity of the tracer particle. Minimising the chance of tracer degradation is important because it would lead to reduced exposure risk and contamination of the fluid medium which would add to the detected noise within the system. The porous nature of the coal made the acceptance of radiolabeling, even for small particle sizes, feasible for long duration tracking relative to the $\lambda_{1/2} = 68$ min half-life of the gallium isotope. The radiation intensity levels of the tracers were sufficient that acceptable levels of activity for tracking remained 2–3 h after tracer generation, as tracer intensity was as high as 2970 μCi, with a mean of 1680 ± 440 μCi.

The determination of the density of the tracer particle presented its own challenges as a standard sink/float analysis would contaminate an untreated coal particle and render it unusable. As such only coated particles were used. At the time, a pycnometer was not available for density determination but will be considered in future experiments. The coating process furthermore introduced both an advantage of increased sphericity of the tracer particle aiding in resistance to breakage as well as an unavoidable variability in the size and density of the tracer. When necessary to achieve relatively high densities, the coating was doped with dense metal shavings, although this also introduced an increase in tracer size. Separate studies are currently being undertaken aimed at finding ways to circumvent these challenges. Table 2 documents the range of tracer sizes and densities as well as medium densities used throughout the experiments.

## 3. Modelling of tangential and axial velocity

The behaviour of fluid within the cyclone is dominated by the tangential velocity component and this shows its largest feature in the radial distribution. For the sake of reference, we shall define the overflow end of the cyclone as "up" and the underflow end as "down". A short synopsis of the prevailing understanding is that the type of vortex seen inside a cyclone breaks down into two radial regions in the idealised case: a central upward moving forced vortex that has increasing tangential velocity with radius which is comparable to solid body rotation; and a free vortex in the outer radial region that has a decreasing tangential velocity towards the inner cyclone wall headed to the underflow. The central upward moving vortex behaves like a solid body rotation, with a linear increase in tangential velocity with increasing radius, described as a "forced" vortex. At the transition point, observed in the PEPT data around the vortex finder radius, the vortex becomes a "free" vortex and follows a power law decay towards the cyclone boundary wall [46]. This relationship can be generalised into the mathematical form of $v_\theta = \frac{C}{r^n}$, where the tangential velocity drops off with radius $r$ and power parameter $n$, for some constant $C$, based on the Alexander model [47]. This environment of large tangential velocity requires larger forces to curve the trajectory of heavier particles, and this leads to the region near the cyclone wall to be crowded out by the particle species with large inertial mass. This forces particles with lower inertia to orbit (on average) at smaller radii. When these orbits are squeezed by the constricting geometry of the cyclone's conical shape extending from the cylindrical part towards the spigot end, the outcome is that the high inertia particles occupy all the space available to exit at the spigot and the low inertia particles are forced into the upwards moving fluid stream towards the vortex finder exit of the cyclone and become the overflow stream.

Based on the calibration experiment of the water-only medium reported as case $D_1$ in this study, the appearance of the bivariate distribution of $v_z$ along the radius $r$ shows a consistent feature. The function at the air core ($R_s$) starts out positive (pointing towards the overflow) and decreases passing through zero and approaches a constant negative value towards the cyclone wall. It seems appropriate to model this feature as a logistic function that blends the opposing axial flow features of the form:

$$v_z(r) = \frac{a}{1 + exp(-b(r - r_0))} + c. \tag{1}$$

Here $a$ represents the height of the logistic function, which corresponds to the axial velocity differential between inner and outer vortex $v_z(R_s) - v_z(R_c)$ and $b$ the steepness of the transition. $r_0$ represents the inflection point of the sigmoid. $c$ represents the axial velocity at the cyclone wall, $v_z(R_c)$. Thus $a$ is proportional to $c$ with an offset equal to the axial velocity at the spigot radius $R_s$, such that $-a = c + \delta$.

In the model proposed in Eq. 1, $a$, $b$, $c$, and $r_0$ are functions of $z$. By definition, $a * c < 0$, where we choose $c < 0$. Examining the model at the radius of zero vertical velocity gives

$$v_z(r_{zvv}) = \frac{a}{1 + exp(-b(r_{ZVV} - r_0))} + c = 0. \tag{2}$$

Rearranging Eq. 2 for the radius of zero vertical velocity gives

$$\Rightarrow r_{ZVV} = r_0 - \frac{1}{b} log\left(\frac{|a + |c||}{c}\right) = r_0 - \frac{1}{b} log\left(\frac{\delta}{c}\right) = r_0 - \frac{1}{b} log\left(\frac{v_z(R_s)}{v_z(R_c)}\right). \tag{3}$$

This model is applied to the experimental data in section 5 where the results are detailed.

## 4. Summary of computational methods

The raw data acquired from the PEPT system were processed in the following order. Firstly, the raw data were triangulated using a sliding window algorithm which, akin to a kernel regression method, determines the region of origin of the gamma ray signal by triangulating multiple lines of response occurring within a range of time intervals determined by the width of the sampling window, and their coincidence is determined to be the location of the tracer particle in three-dimensional space. This sampling window then moves along the

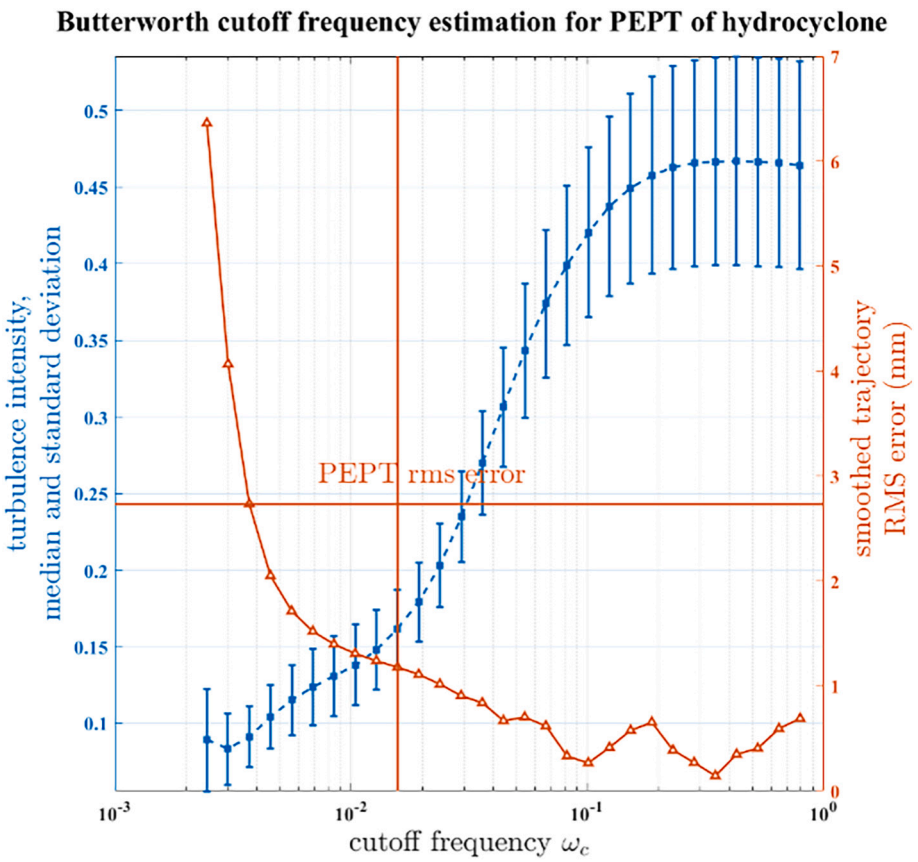


**Fig. 3.** Cut-off frequency response of turbulence intensity (blue curve) and error deviation of filtered tajectorys (orange curve), for the water-only medium tracking experiment. The mean squared error of the filtered trajectory was determined to be appropriate, if it fell below the triangulation error range (orange dashed lines), giving a normalised cut-off frequency of $2.5 \times 10^{-2}$.

timeline of acquired LoRs in an overlapping fashion to build a set of trajectory points. This overlapping sampling ensures that the triangulation of the signal is performed with a large enough data set to reduce noise within the system by making large outliers less significant, thereby generating smoother trajectories, and improving the determination of derivatives such as velocity and its variance. This is important for a PEPT experiment involving a tracer within the high noise environment of a cyclone as it trades a small increase in the error inherent in the tracer's location with lower variation in the higher order derivatives. Alongside the traditional triangulation method as detailed in [45] these processing algorithms will generate data of both high accuracy location as well as reduced noise to make determinations about separation mechanisms based on velocity and turbulence estimates. This feature of the sliding window approach will be used when referring to velocity data.

The optimisation of the triangulation method involves the tuning of two parameters $f_{opt}$ and $N_{lines}$ which set the minimum fraction of retained lines of response and the total number of lines of response to process within a given time frame, as set out in [45]. Once a set of trajectory coordinates are determined through triangulation for a range of the parameters $f_{opt}$ and $N_{lines}$, these are processed to find the set with lowest RMS error in location, yielding the optimised data set.

This set of locations is then filtered to exclude outliers of unphysically large velocity values by searching for outlier time gaps within the data series. A Butterworth low-pass filter of 2nd order is applied to the trajectory data to filter out higher order frequencies, with a normalised cut-off frequency of $1.57 \times 10^{-2}$, determined such that the filtered and phase-corrected trajectory data does not deviate from the triangulated trajectory data by more than the error that results from the triangulation scheme of PEPT and minimise the variance of the trajectory turbulence intensities. The RMS errors relative to the raw trajectory data and spectrum of turbulence excluded by this approach are detailed in Fig. 3 alongside. The control case of D1, the tracer in water-only medium, was used to determine this Butterworth cut-off frequency, thereby calibrating the turbulence intensity (coefficient of variation of velocity) for the dense medium tracer experiments. Subsequently the trajectory data are interpolated using the Savitzky-Golay 2nd order polynomials with sampling window of 5 locations) which have been shown to give best fit while preserving the shape of the trajectory [20] and from which derivatives are estimated.

Bivariate distributions are sampled with a similar “sliding window” technique using kernel regression with a default localness parameter. This parameter determines the size of the window relative to the range of the sampling variable. For instance, a localness of $l = 3$ results in a sampling width fraction of $K_w$ $(l = 3) = 2^{l-7} = 2^{-4} = 1/16$ times the width of the entire range of data. For instance, when a radial quantity is sampled between $r$= 0 and $R_{cyc}$=0.05 m, 25 bins with a localness of 3 (to represent the best-case spatial resolution of the Siemens EXACT3D), leads to a set of sampling bins with overlap of 50% in adjacent bins compared to a localness of 1.356 which has no overlap with no gaps in sampling (standard histogram sampling). This optimised localness enables reasonable suppression of local noise within the data by sampling from sufficient data points and allows resolution of the underlying distribution of kinematic flow quantities without aggressively smoothing the data to an extent where some key features of the data are masked.

For the axial-radial distribution visualisation in a cylindrical coordinate system, the full three-dimensional data set is divided into two equal angular regions (half-cylinders) and each two-dimensional rectangle on a distribution map represents the data sampled from a semi-toroidal shaped volume, thus mapping the full space onto a two-dimensional plane [48] and giving a representation as shown in

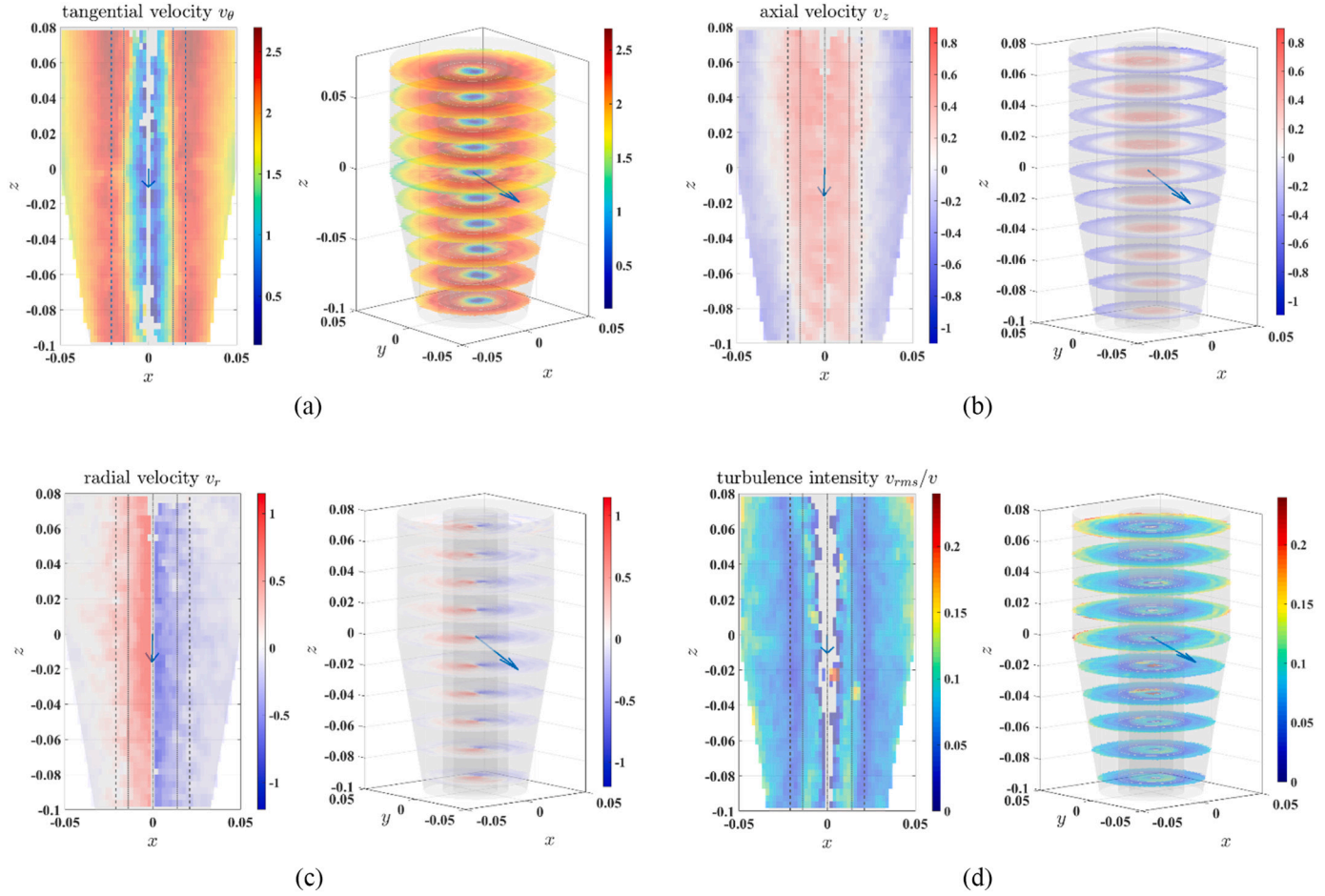


**Fig. 4.** (a): Tangential velocity $v_\theta$ (m/s) map for a neutrally buoyant tracer in dense medium, D5_1. Fig. 4(b): Axial velocity $v_z$ (m/s) map for a neutrally buoyant tracer in dense medium. The effect of gravity on the inner vortex (red shaded region) can be seen on the right. Fig. 4(c): Radial velocity $v_r$ map for a neutrally buoyant tracer in dense medium. The distribution shows angular regions of clear outward and inward radial motion, jets of expulsion from the inner vortex (red). The orientation of these regions changes after the transition to the conical section. Fig. 4(d): Turbulence intensity map for a neutrally buoyant tracer in dense medium. The "shadow" of the vortex finder (radius indicated as dashed lines) can be seen on the left as parallel lines of minimal turbulence and on the right as concentric rings of dark blue, along the axis of the cyclone, bounding the inner vortex.

Figs. 4(a) and (b) in the next section. This implies volumes of the outer voxels need to be adjusted accordingly when densities are considered.

The estimation for the turbulence intensity [49], defined as the coefficient of variation, i.e., ratio of root-mean-square velocity and the time averaged mean velocity - is made using a normal distribution linear regression fit to the velocity distribution, from which mean, and variation are determined for the tracer NGM particles in a DMC.

## 5. Results

Examples of the tangential, axial, and radial velocity fields $v_\theta$, $v_z$, $v_r$ as well as the turbulence intensity of a neutrally buoyant tracer to show the maximal coverage of the cyclone volume within the field of view of the PEPT scanner are given in Figs. 4(a), (b), (c), and (d), respectively. The tangential velocity map in Fig. 4(a) shows the power law behaviour of the outer free vortex as a smooth transition from red to yellow/green colour. The axial velocity map in Fig. 4(b) illustrates the locus of zero axial velocity $r_{ZVV}$ as a white band between the upward moving central red zone of the forced vortex and the downward moving blue zone of the free vortex.

The radial velocity map of Fig. 4(c) shows one half of the inner vortex prone to ejecting tracers from within the upward moving stream while the other half has, on average, radially inward moving particles. This suggests a more complex circulation pattern worth further investigation.

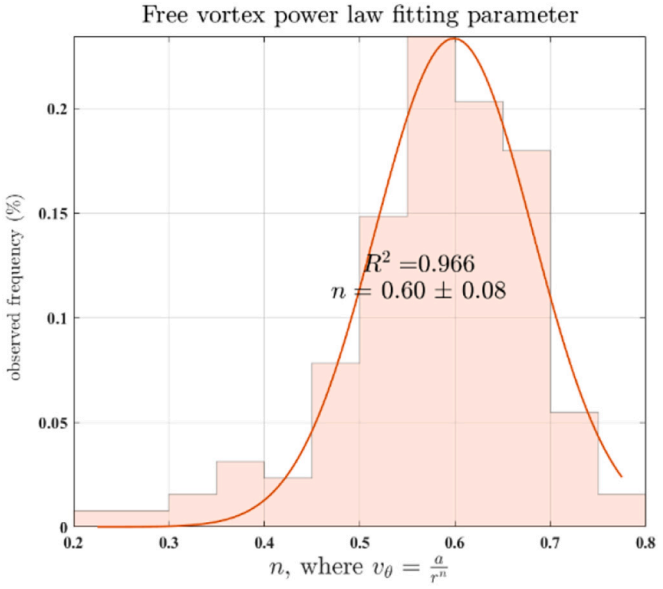


**Fig. 5.** Distribution of power fitting parameter of tangential velocity of free vortex.

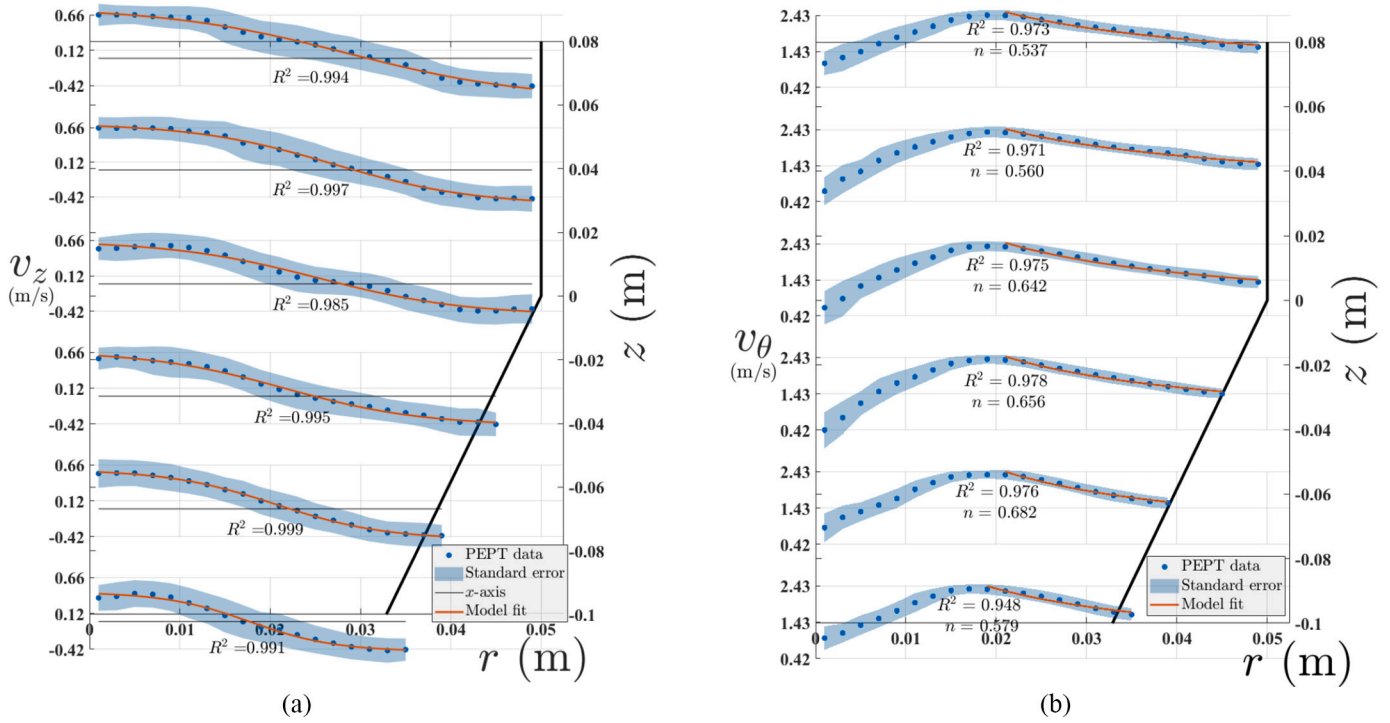


**Fig. 6.** (a): Axial velocity as a function of radius, along the axial dimension of the cyclone, showing the locus of zero axial velocity (curve intersections with axes) (from data set D12 as shown in Table 2). Fig. 6(b): Tangential velocity profiles $v_\theta$ versus radius $r$, along the axial dimension $z$. The power law decay fits the free vortex in the outer radial region well. The forced vortex is also apparent near the central region. On average for all tracers, $n = 0.60 \pm 0.08$ (from data set D12 as shown in Table 2).

The map of turbulence intensity, the ratio of velocity fluctuations to mean velocity or coefficient of variation of velocity, shown in Fig. 4(d), reveals the turbulence "shadow" cast by the vortex finder where the turbulent motion is minimal as can be identified by lines of dark blue parallel to the central vortex on the left-hand image and concentric circles of dark blue on the right-hand image.

### 5.1. Radial profiles of axial and tangential velocity

The Rankine vortex model description of the cyclone system mentioned in Section 3 is also observed in this data. The power law exponent is calculated to be $n = 0.60 \pm 0.08$ on average for all tracers throughout the imaged volume. The distribution of tangential velocity decay exponents is shown in Fig. 5. The denser tracers have low

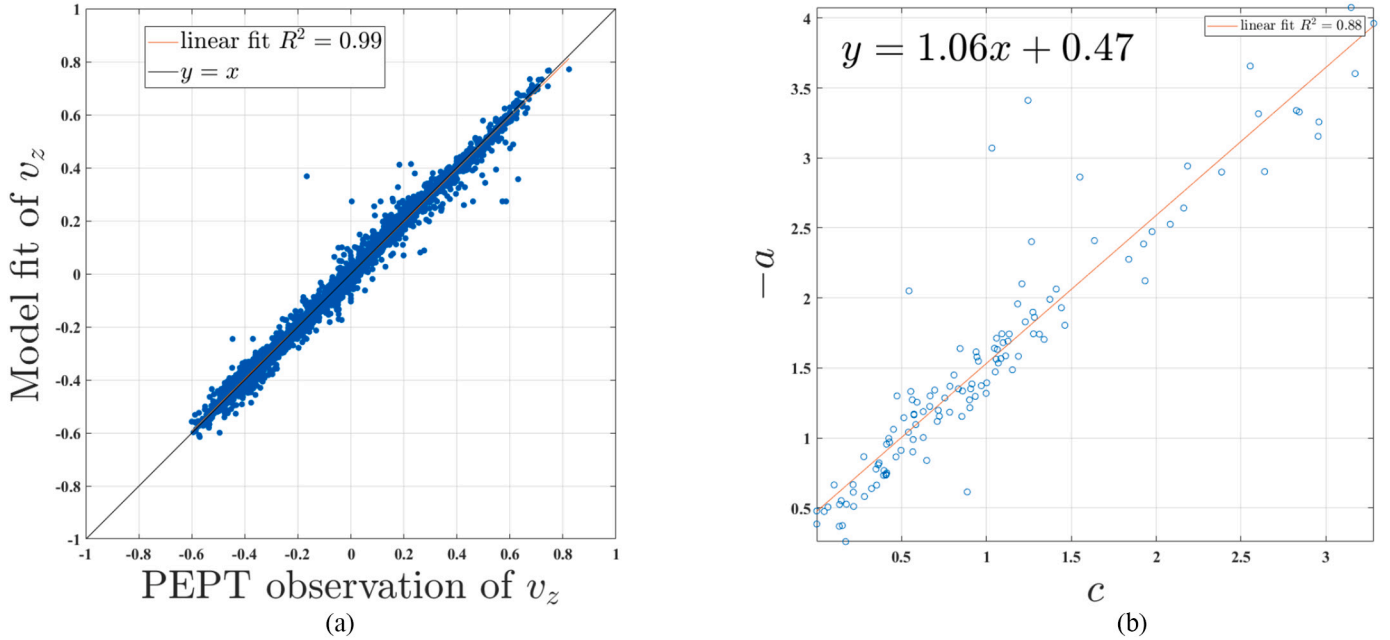


**Fig. 7.** (a): Axial velocity model logistic function fit to PEPT observational data located between the spigot and cyclone radius. Fig. 7(b): relationship between axial velocity model function parameters a and c showing proportionality with constant offset.

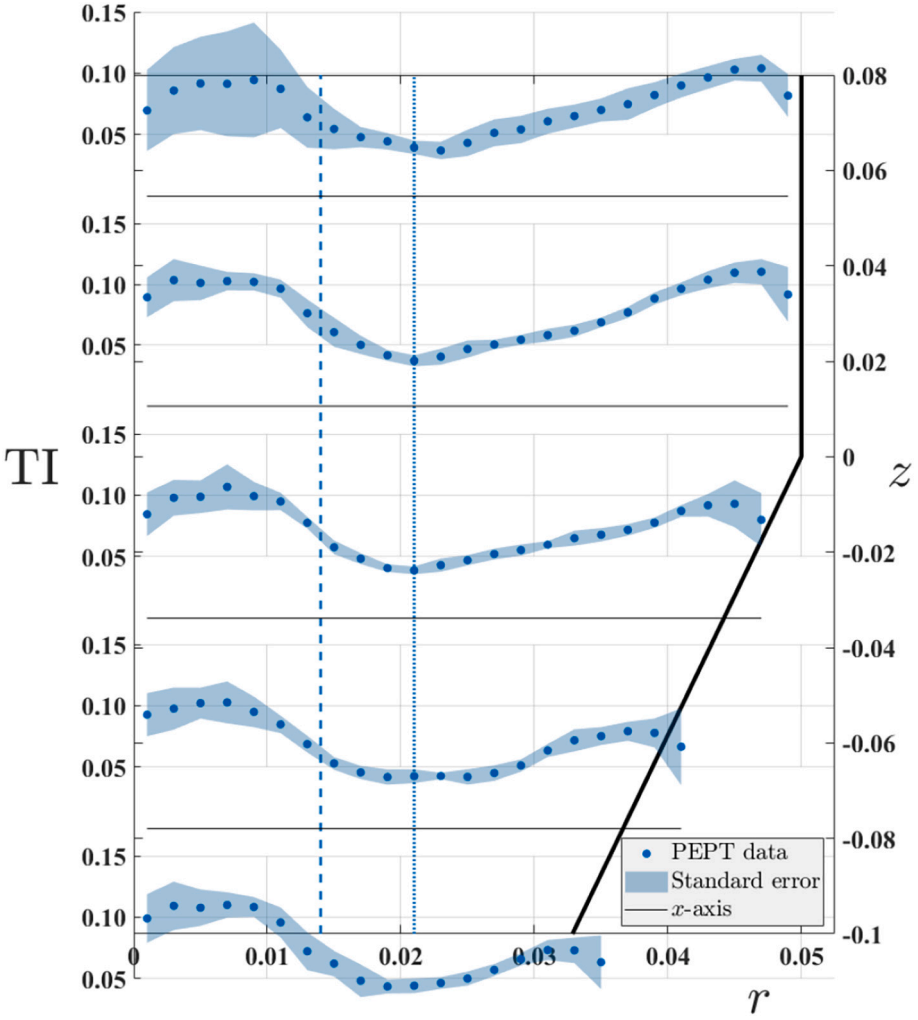


**Fig. 8.** Radial turbulence profile for a neutral buoyancy tracer along the axial dimension segments of the dense media cyclone (from data set D12 as shown in Table 2). Dashed and dotted lines represent the spigot and vortex finder radii respectively.

occupancy in the central region and provide little data in verifying the forced vortex region. The less dense and neutrally buoyant tracers map the region where the linear forced inner vortex is to be expected and thus far less information about this region is captured in this study as these tracers tended to disintegrate more easily. The power law decay of the free vortex tangential velocity along the radial direction is strongly indicated with low residual variation in the fit decay curve, as can be seen in Fig. 6(b), due to high occupancy in the outer radial region. We observe that $n$ seems to trend higher around and beyond the cylinder/cone transition point ($z = 0$) of the cyclone, although this is not shown to be statistically significant on account of the overlap in uncertainty. On average for all tracers, $n_{cyl} = 0.58 \pm 0.05$ while $n_{cone} = 0.62 \pm 0.09$. The driven vortex region was poorly sampled overall due to the overly dense tracers having a higher representation among the successful tracers, and thus a study-wide determination of the linearly increasing velocity profile is not attempted. This may tell us something about the forces present in driven vortex region that act on the tracer making breakage of a less dense particle more probable, however this is based on too small a sample size to be conclusive.

The axial velocity profile as a function of radius as acquired with PEPT in Fig. 6(a) shows the transition of the upward moving inner forced vortex through the locus of zero axial velocity (also termed the locus of zero vertical velocity) $r_{ZVV}$ to the downward moving outer free vortex. This relationship can be modeled as a logistic function, which fit the data consistently. The shapes of both axial and tangential velocity components in the radial dimension are in broad agreement with other tracking studies on cyclonic velocity profiles such as shown in [50].

Applying this logistic axial velocity model form to the dense medium experimental data yields good agreement with trajectory data as shown in Fig. 6(a) and 7(a). Furthermore, the condition of the parameter relations of the parameters $a$ and $c$ show the desired consistency and proportionality as seen in Fig. 7(b).

### 5.2. Turbulence

The radial distribution of turbulence intensity (TI) shown in Fig. 8 shows the general trend of the tracers imaged with PEPT. All tracers display the features of turbulence near the cyclone wall, of linearly decreasing turbulence intensity when moving closer to the inner vortex. Most tracers produced a local minimum of turbulence as observed in Fig. 8, typically. The consistent feature among those tracers displaying this turbulence minimum, is the location of this zone of coinciding with the radius of the vortex finder (dotted line in Fig. 8). When no local minimum was present in the turbulence radial profile the trend was linearly decreasing from the cyclone wall inwards, until a transition to a steeper turbulence slope towards the center of the cyclone. Subtle differences arise when comparing tracers of varying density relative to the feed density as not all tracers produced this local minimum turbulence zone. The overall distribution of inferred turbulence recorded with PEPT as shown in Fig. 9, reveals a long-tailed distribution for all coal slurry

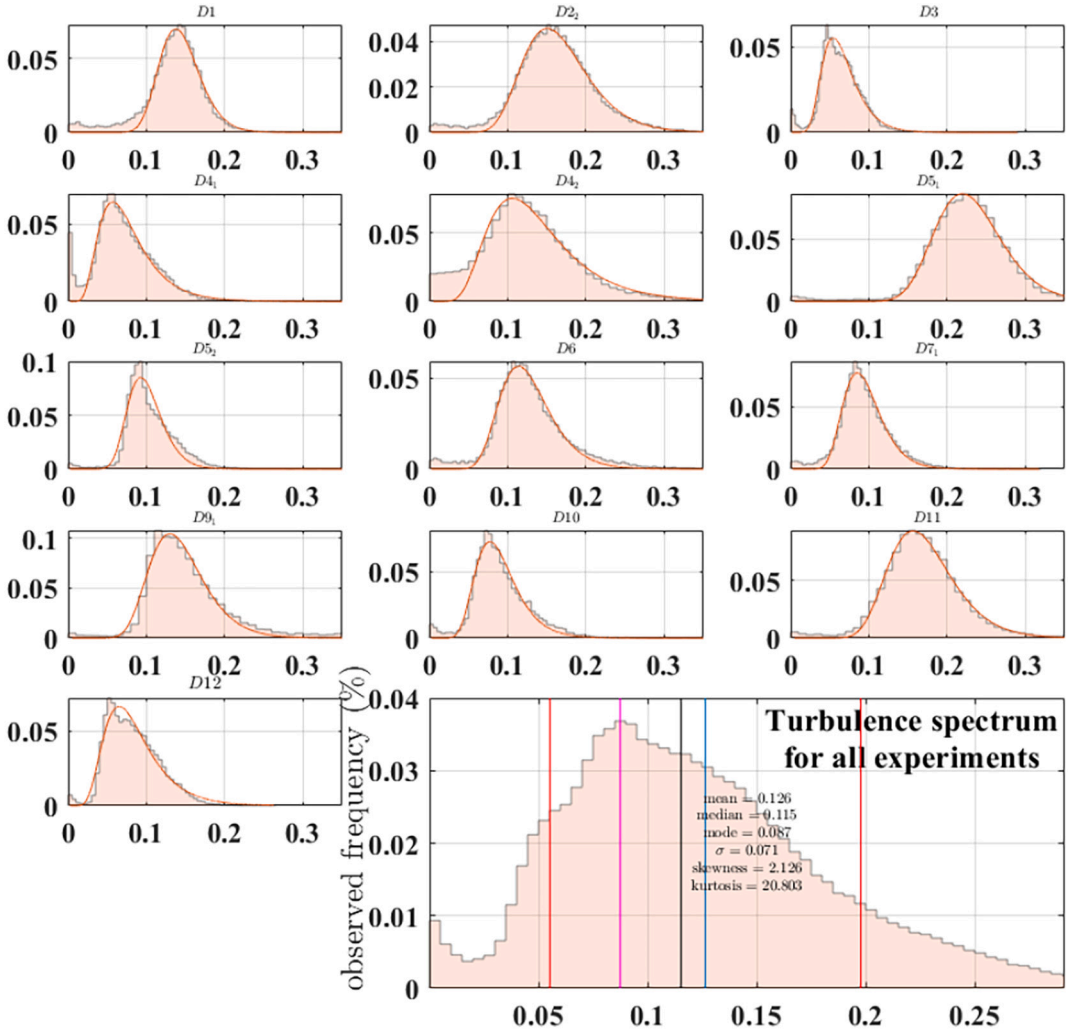


**Fig. 9.** Turbulence distributions for the single particle tracer experiments. While the water-only medium case shows a near normal distribution, the general feature of the dense medium cyclone trajectories is a long-tailed distribution of turbulence values, better fitting a lognormal distribution.

medium experimental cases. The control of water- medium shows a turbulence distribution more closely resembling a normal distribution.

### 5.3. Underflow reporting probability

The probability of a tracer reporting to the underflow was determined from the trajectory data over the course of the total tracking time, here referred to as the underflow reporting probability (URP), is a PEPT-observed metric determined by counting the underflow exits of the tracer as a ratio of total number of field-of-view traversals. This probability was correlated with the radial distance between the tracer's mean radial location $r_{modal}$ and the radial locus of zero axial velocity $r_{ZVV}$ (commonly referred to as the locus of zero vertical velocity). The mean radial distance between particle and the separation zone $r_{ZVV}$ is shown for the three varieties of tracer density as well as the control case in Fig. 10 and the correlation of this gap with observed ratio of tracers reporting to the underflow is shown in Fig. 11. This relationship indicates that a particle's relative proximity to the zone of zero axial velocity influences the probability of it reporting to the underflow, with larger separations away from the $r_{ZVV}$ and towards the cyclone wall having a larger probability of being captured in the underflow stream.

## 6. Conclusions

A particle tracking study of near-gravity activated coal particles circulating in a dense medium cyclone system has been presented. Various location probability and velocity distributions of tracers of varying relative density to the feed and a range of particle sizes in a magnetite and coal bearing medium pushed through a dense medium cyclone operating at optimum pressure were presented. The locus of zero vertical velocity is imaged as a time average. The tangential velocity distribution as a function of radius demonstrated a free vortex profile that fits a power law decay trend towards the cyclone wall with fitted power parameter of $n = 0.60 \pm 0.08$. A logistic model of the axial velocity trend as function of radius around the locus of zero axial velocity, based on observations of the control experiment in water, showed good agreement with the PEPT data of the dense medium tests. The cyclone separation efficiency was shown to correlate with the tracer's modal separation from the locus of zero axial velocity. Turbulence estimates of the various tracers were presented, showing the region of minimal turbulence intensity and quantifying the majority of the turbulence distribution within the range of 0.05 to 0.20. The radial velocities, although showing high variance proportional to the mean, were shown to exhibit consistent and distinct angular features which require further study.

This demonstrates the useful nature of PEPT in imaging opaque systems and generating trajectory level and time averaged data for statistical analysis of dynamical systems and theoretical and numerical model validation for complex systems such as cyclones and particularly DMCs. The favourable comparison of the radial profile of turbulence

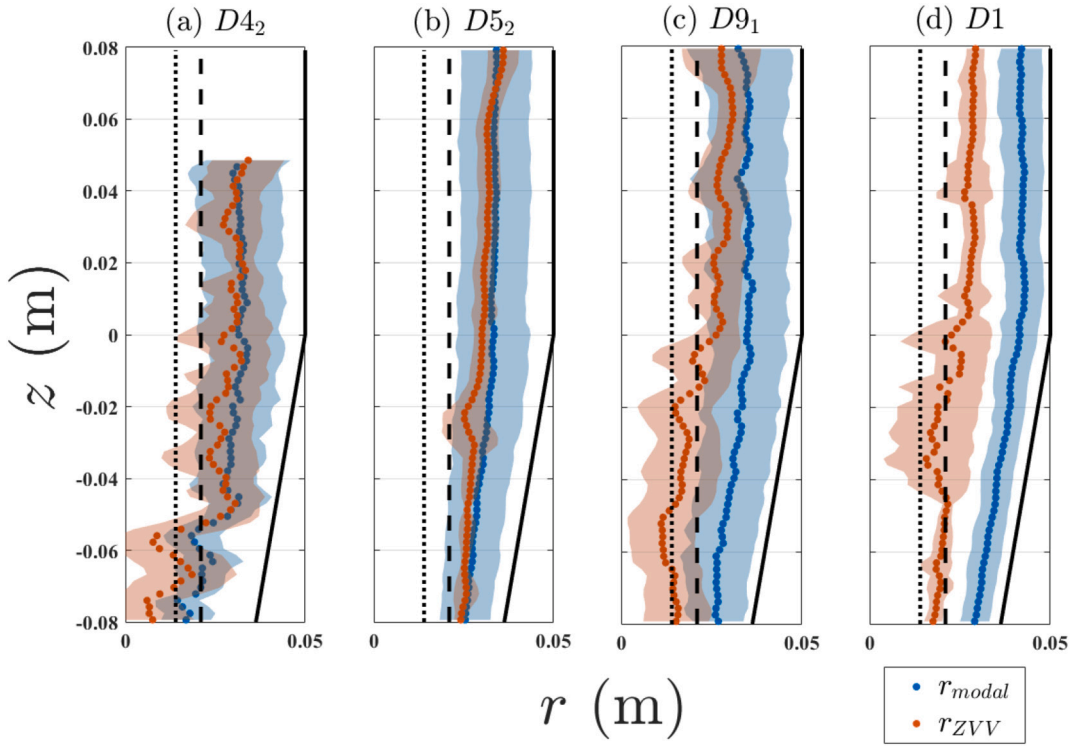


**Fig. 10.** Median radial tracer location $r_{median}$ compared to radial locus of zero axial velocity $r_{ZVV}$ for 4 distinct tracers. (a) less dense than the medium, (b) neutrally buoyant, (c) denser than the medium, and (d) is the control case with water-only medium. Dotted and dashed lines represent the spigot and vortex finder radii respectively.

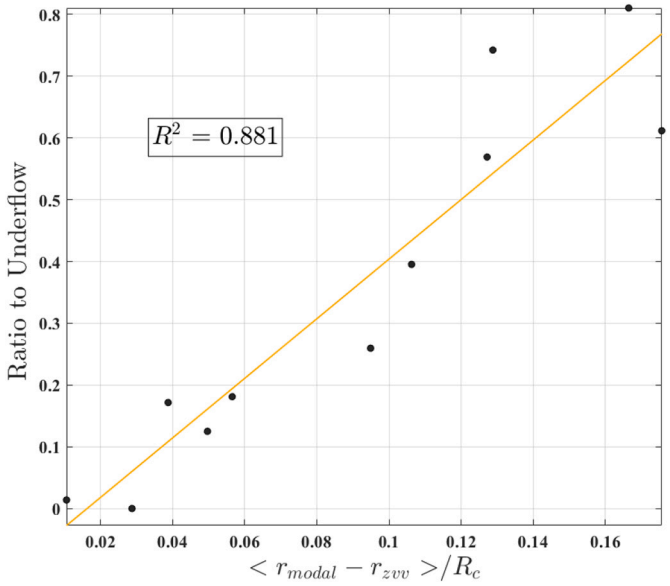


**Fig. 11.** Cyclone separator efficiency correlates with separation of modal radius to radial locus of zero axial velocity $\langle r_{modal} - r_{ZVV} \rangle$.

intensity shows agreement with CFD simulation results lending validity to the numerical work capable of investigating further points of improvement with turbulence estimation aiding DMC design improvements. Further potential work on this topic would have to include a more comprehensive multi-particle tracking application and further empirical study of the cyclone separation efficiency in situ, with appropriate safety precautions to mitigate contamination risk.

## CRediT authorship contribution statement

**M.C. Richter:** Writing – original draft, Data curation, Investigation, Software, Formal analysis, Visualization, Project administration. **A.N. Mainza:** Conceptualization, Supervision, Writing – review & editing. **I. Govender:** Supervision, Conceptualization, Writing – review & editing. **N. Mangadoddy:** Conceptualization, Supervision, Writing – review & editing. **R. Sivakumar:** Investigation. **G.E. Sreedhar:** Investigation. **M. R. van Heerden:** Investigation, Methodology, Resources.

## Declaration of Competing Interest

The authors declare that they have no known competing financial interests or personal relationships that could have appeared to influence the work reported in this paper.

## Data availability

Data will be made available on request.

## Appendix A. Supplementary data

Supplementary data to this article can be found online at https://doi.org/10.1016/j.powtec.2022.118095.

## References

[1] A.N. Mainza, N. Mangadoddy, M.S. Powell, P.N. Holtham, M.S. Brennan, Study of flow behaviour in three-product cyclone using computational fluid dynamics, Miner. Eng. 19 (2006) 1048–1058.
[2] N. Mangadoddy, A.N. Mainza, P.N. Holtham, M.S. Powell, M.S. Brennan, A semi-mechanistic model of hydrocyclones - developed for industrial data and inputs from CFD, Int. J. Miner. Process. 133 (2014) 1–12.
[3] T. Napier-Munn, The dense medium cyclone - past, present and future, Min. Eng. 116 (2018) 107–113.

[4] R.O. Burt, C. Mills, Gravity Concentration Technology, Developments in Minerals Processing, Elsevier, Amsterdam, 1984.
[5] B.A. Wills, J. Finch, Wills' Minerals Processing Technology: An Introduction to the Practical Aspects of Ore Treatment and Mineral Recovery, Butterworth-Heinemann, 2015.
[6] C.J. Wood, A Performance Model for Coal-Washing Dense Medium Cyclones, 1990.
[7] M. Dungilson, A model to preduct the performance of the dense medium cyclone for low and high density applications, in: *Seventh JKMRC Conference*, Brisbane, Australia, 1998.
[8] R.-M. Lim, Y.-R. Chen, C.-H. Wang, E.W. Wu, Experimental and computational studies of multiphase hydrocyclone separator system, Chem. Eng. Sci. 65 (2010) 6415–6424.
[9] M.J. Fisher, D. Flack, Velocity distribution in a hydrocyclone, Exp. Fluids 32 (2002) 302–312.
[10] K.T. Hsieh, K. Rajamani, Phenomenological model of the hydrocyclone: model development and verification for single-phase flow, Int. J. Miner. Process. 22 (1988) 223–237.
[11] M. Barigou, Particle tracking in opaque systems: an overview of the capabilities of PET and PEPT, Chem. Eng. Res. Des. 82 (2004) 1258–1267.
[12] M. Marigo, M. Davies, T. Leadbeater, D.L. Cairns, A. Ingram, E.H. Stitt, Application of positron emission particle tracking (PEPT) to validate a discrete element method (DEM) model of granular flow and mixing in the turbulence mixer, Exp. Fluids 446 (2013) 46–58.
[13] M. Van de Velden, J. Baeyens, J.P.K. Seville, X. Fan, The solids flow in the riser of a circulating fluidised bed (CFB) viewed by positron emission particle tracking (PEPT), Powder Technol. 183 (2008) 290–296.
[14] L.S. Bbosa, I. Govender, A.N. Mainza, M.S. Powell, Power draw estimations in experimental tumbling mills using PEPT, Miner. Eng. 24 (2011) 319–324.
[15] T.S. Volkwyn, A. Buffler, I. Govender, J.-P. Franzidis, A.J. Morrison, A. Odo, N. P. van der Meulen, C. Vermeulen, Studies of the effect of tracer activity on time-averaged positron emission particle tracking measurements on tumbling mills at PEPT Cape Town, Miner. Eng. 24 (2011) 261–266.
[16] K.E. Cole, K.E. Waters, X. Fan, S.J. Neethling, J.J. Cilliers, Combining positron emission particle tracking and image analysis to interpret particle motion in froths, Miner. Eng. 23 (2010) 1036–1044.
[17] K.E. Waters, N.A. Rowson, X. Fan, D.J. Parker, J.J. Cilliers, Positron emission particle tracking as a method to map the movement of particles in the pulp and froth phases, Miner. Eng. 21 (2008) 877–882.
[18] Y.-F. Chang, C.G. Ilea, L. Aasen, A.C. Hoffmann, Particle flow in a hydrocyclone investigated by positron emission particle tracking, Chem. Eng. Sci. 66 (2011) 4203–4211.
[19] J.R. Radman, R. Langlois, T. Leadbeater, J. Finch, N. Rowson, K. Waters, Particle flow visualization in quartz slurry inside hydrocyclone using the positron emission particle tracking technique, Miner. Eng. 62 (2014) 142–145.
[20] Y.-F. Chang, A.C. Hoffmann, A Lagrangian study of liquid flow in a reverse-flow hydrocyclone using positron emission particle tracking, Exp. Fluids 56 (2015) 4.
[21] G. Fanglu, L. Wenzhen, Measurement and study of velocity field in various cycloines by use of laser doppler anemometry, in: Proceedings of 3rd International Conference of Hydrocyclones, England, Oxford, 1987.
[22] K.P. Galvin, J.B. Smitham, Use of X-rays to determine the distribution of particles in an operating cyclone, Min. Eng. 7 (1994) 1269–1280.
[23] V.J. Subramanian, Measurement of Medium Segregation in the Dense Medium Cyclone Using Gamma-Ray Tomography, PhD thesis, University of Queensland, JKMRC, 2002.
[24] M.E. Dungilson, A model to predict the performance of the dense medium cyclone for low and high density applications, in: *7th JKMRC Conference*, Brisbane, Australia, 1998.
[25] C.J. Wood, A Performance Model for Coal-Washing Dense Medium Cyclones, PhD Thesis, JKMRC, University of Queensland, 1990.
[26] M.I.G. Bloor, D.B. Ingham, The flow of industrial cyclones, J. Fluid Mech. 178 (1987) 507–529.
[27] F. Boysan, B.C.R. Ewan, J. Swithenbank, W.H. Ayers, Experimental and theoretical studies of cyclone separator aerodynamics, in: Institute of Chemical Engineering Symposium Series, 1983.
[28] D. Gao, J.A. Herbst, Alternative ways of coupling particle behaviour with fluid dynamics in mineral processing, Int. J. Comp. Fluid Dyn. 23 (2) (2009) 109–118.
[29] H.D. Zughbi, M.P. Schwaz, W.J. Turner, W. Hutton, Numerical and experimental investigations of wear in heavy medium cyclones, Min. Eng. 4 (1991) 245–262.
[30] D.J. Suasnabar, C.A.J. Fletcher, CFD simulation of dense medium cyclones, in: Proceedings of the 13th Australasian Fluid Mechanics Conference, 1998.
[31] M.S. Brennan, P.N. Holtham, R. Rong, G.J. Lyman, Computational fluid dynamic simulation of dense medium cyclones, in: *Proceedings of the 9th Australian Coal Preparation Conference*, Yeppoon, Australia, 2002.
[32] M. Manninen, V. Taivassalo, S. Kallio, On the Mixture Model for Multiphase Flow, VTT Publications, Finland, 1996.
[33] M. Narasimha, M.S. Brennan, P.N. Holtham, Prediction of magnetite segregation in dense medium cyclone using computational fluid dynamics technique, Int. J. Miner. Process. 82 (2007) 41–56.
[34] M. Ishii, K. Mishima, Two-fliud model and hydrodynamic constitutive relations, Nucl. Eng. Des. 82 (1984) 107–126.
[35] B. Wang, K.W. Chu, A.B. Yu, A. Vince, Modelling the multiphase flow in a dense medium cyclone, Ind. Eng. Chem. Res. 48 (2009) 3628–3639.
[36] K.W. Chu, B. Wang, A.B. Yu, A. Vince, G.D. Barnett, P.J. Barnett, CFD-DEM study of the effect of particle density distribution on the multiphase flow and performance of dense medium cyclone, Powder Technol. 193 (2009) 235–247.
[37] K. Chu, B. Wang, A. Yu, A. Vince, G. Barnett, P. Barnett, CFD-DEM study of the effect of particle density distribution on the multiphase flow and performance of dense medium cyclone, Min. Eng. 22 (11) (2009) 893–909.
[38] K. Chu, J. Chen, B. Wang, A. Yu, A. Vince, G. Barnett, P. Barnett, Understand solids loading effects in a dense medium cyclone: effect of particle size by CFD-DEM method, Powder Technol. 320 (2017) 594–609.
[39] K. Chu, S. Kuang, A. Yu, A. Vince, Particle scale modelling of the multiphase flow in a dense medium cyclone: effect of fluctuation of solids flowrate, Min. Eng. 33 (2012) 34–45.
[40] T.R. Vakamalla, M. Narasimha, Rheology-based CFD modelling of magnetite medium segregation in a dense medium cyclone, Powder Technol. 277 (2015) 275–286.
[41] M. Kumar, N. Mangadoddy, R. Banerjee, G.E. Sreedhar, S.K. Raparla, R. Kumar, Hydrodynamic force analysis of magnetite medium inside dense medium cyclone using multiphase GPU parallelized ASM model, Min. Eng. 170 (2021).
[42] J.W. Leonard, Coal preparation, AIME 4 (1979) 30.
[43] G.J. Sanders, The Principles of Coal Preparation 4, 2007, p. 130.
[44] G.J. De Korte, Int. J. Coal Preparat. Utilit. 28 (2008) 69.
[45] D.J. Parker, P. Fowles, M.R. Hawkesworth, P. McNeil, C.J. Broadbent, Positron emission particle tracking - a technique for studying flow within engineering equipment, in: *Nuclear Instrumentation and Methodologicl* Physics 326, 1993, pp. 592–607.
[46] D. Bradley, The Hydrocyclone, Pergamon Press, Oxford, 1965.
[47] R.M. Alexander, Fundamentals of cyclone design and operation, Proc Aust Inst Min Metall 152 (1949) 203–228.
[48] F. Chiti, S. Bakalisa, W. Bujalskia, M. Barigoua, A. Eagleshamb, A.W. Nienowal, Using positron emission particle tracking (PEPT) to study the turbulent flow in a baffled vessel agitated by a Rushton turbine: improving data treatment and validation, Chem. Eng. Res and Des. 89 (2011) 1947–1960.
[49] R.D. Wildman, J.M. Huntley, J.-P. Hansen, D.J. Parker, D.A. Allen, Single motion in three-dimensional vibro-fluidized granular beds, Phys. Rev. E 62 (2000) 3826–3835.
[50] B. Chiné, F. Concha, Flow patterns in conical and cylindrical hydrocyclones, Chem. Eng. J. 80 (2000) 267–273.